ORIGINAL PAPER

Density functional study of oxygen vacancy formation and spin density distribution in octahedral ceria nanoparticles

Talgat M. Inerbaev · Sudipta Seal · Artëm E. Masunov

Abstract We report plane wave basis density functional theory (DFT) calculations of the oxygen vacancies formation energy in nanocrystalline CeO_{2-x} in comparison with corresponding results for bulk and (111) CeO_2 surface. Effects of strong electronic correlation of Ce4f states are taken into account through the use of an effective on-site Coulomb repulsive interaction within DFT+U approach. Different combinations of exchange-correlation functionals and corresponding U values reported in the literature are tested and the obtained results compared with experimental data. We found that both absolute values and trends in oxygen vacancy formation energy depend on the value of U and associated with degree of localization of Ce4f states. Effect of oxygen vacancy and geometry optimization method on spatial spin distribution in model ceria nanoparticles is also discussed.

Keywords Cerum dioxide · Density functional theory · DFT+U · Nanoceria · Nanoparticles · Oxygen vacancy

T. M. Inerbaev · S. Seal · A. E. Masunov (✉)
NanoScience Technology Center, University of Central Florida,
12424 Research Parkway, Ste 400,
Orlando, FL 32826, USA
e-mail: amasunov@mail.ucf.edu

S. Seal
Department of Mechanical, Material and Aerospace Engineering,
University of Central Florida,
4000 Central Florida Blvd., Eng 381,
Orlando, FL 32816, USA

S. Seal
Advanced Materials Processing and Analysis Center,
University of Central Florida,
4000 Central Florida Blvd., Eng 381,
Orlando, FL 32816, USA

A. E. Masunov
Department of Chemistry, University of Central Florida,
4000 Central Florida Blvd., CH 117,
Orlando, FL 32816, USA

A. E. Masunov
Department of Physics, University of Central Florida,
4000 Central Florida Blvd., MAP 310,
Orlando, FL 32816, USA

A. E. Masunov
Florida Solar Energy Center, University of Central Florida,
1679 Clearlake Road,
Orlando, FL 32816, USA

Introduction

Cerium is a rare earth element, the first in lanthanide series. Cerium oxide, or ceria, is technologically important material with remarkable properties that is used in a number of applications. Major applications of ceria are in catalysis [1] and solid oxide fuel cells [2]. The unique property of ceria nanoparticles in radical scavenging makes it a high promising material for biomedical applications [3].

Bulk cerium oxide has two stable stoichiometric forms: the cubic [4] fluorite-type dioxide (CeO_2) $Fm3m$ and the hexagonal [5] cerium sesquioxide (Ce_2O_3) $P\bar{3}m$. In these compounds Ce atoms have +4 and +3 oxidation states respectively. In Ce_2O_3 one electron per cation occupies the Ce4f subvalent orbital, which remains empty in CeO_2. Close thermodynamic stability of these stoichiometric forms leads to continuous range of partially reduced (also called "mixed valence") phases CeO_{2-x}, where oxygen vacancy (V_O) can be easily formed or eliminated [6]. This "oxygen storage capacity" of ceria is well known and is widely used in a number of catalytic processes, most notably for purification of exhaust gases in three-way

automotive catalytic converters [7, 8]. The formation of oxygen vacancies in CeO_{2-x} results in the change in cerium oxidation state [9, 10]. The valence and defect structure of ceria is dynamic and may change in response to physical parameters such as temperature, presence of other ions, and oxygen partial pressure [9, 11, 12]. Nanocrystalline form of ceria was shown to increase the oxygen vacancy concentration with the decrease of particle size [13, 14]. Measurements of defect formation energy revealed that for nanoceria heat of reduction is by a factor of 2 lower than the corresponding single crystal value [15–17]. Thus, defect thermodynamics of nanoceria significantly differs from the bulk material.

Qualitatively correct and internally consistent computational description of cerium oxides in both oxidation states presented a challenge for electronic structure approaches. The computational description of perfect CeO_2 structure is not so complicated due to the absence of $Ce4f$ electrons. Density functional theory (DFT) calculations somewhat underestimate the band gap value [18–20], which is a general drawback of pure DFT. However, for insulating Ce_2O_3 standard DFT calculations fail to reproduce the localized nature of of $Ce4f$ electrons and predict the band structure that corresponds to a metallic state [18, 20, 21]. These shortcomings may be eliminated in advanced DFT approaches including: (i) addition of semiempirical or self-consistent Hubbard parameter U to take into account on-site electron correlations (DFT+U method) [19, 22–25], (ii) self-interaction-corrected DFT (SIC-DFT) [26, 27], and (iii) hybrid Hartree-Fock/DFT approach [28, 29].

Hybrid functionals, that include a fraction of the Hartree-Fock exchange, provide a reasonably balanced description of lattice constants and optical properties of both CeO_2 and Ce_2O_3 [28, 29], while the relative energetics is predicted less accurately [29]. Due to lower computational cost, DFT+U approach is used to study ceria more often [19, 20, 22, 25, 29–36]. This method presents the simplest form of the orbital-dependent exchange-correlation functional and has two parameters for each atomic orbital: the Hubbard parameter U (which reflects the strength of on-site Coulomb interaction), and parameter J (which adjusts the strength of the exchange interaction). In the simplified rotationally invariant method due to Dudarev et al. [37], these parameters are combined into a single parameter $U_{eff} = U\text{-}J$. This parameter, determined self-consistently for $Ce4f$ orbital by Cococcioni et al. [31] amounts to U_{eff}=2.5–3.5 eV for local density approximation (LDA) and U_{eff}=1.5–2.0 eV for gradient-generalized approximation (GGA) in Perdew-Burke-Ernzerhof (PBE) parametrization. However, semi-empirical adjustment of U_{eff} to fit certain observables to their experimentally determined values proved to be a more practical approach. For instance, the value of U_{eff}= 6.3 eV combined with PBE functional was found to give a

better agreement with experiment for equilibrium lattice constant and elastic bulk moduli [33].

A number of papers discuss appropriate U values for both LDA and GGA methods [20, 22, 25, 29, 30, 32, 36, 38]. Surprisingly, LDA+U approach describes geometry and thermodynamics of both cerium oxides forms more accurately than GGA+U one [22, 25]. Loschen et al. argued [22] that thermodynamic properties of ceria are reproduced more accurately by LDA+U due to fortuitous error cancellation and it is more rigorous to use GGA+U approach. Da Silva et al. suggested [29] values of U_{eff}= 2.0 eV (for PBE) and U_{eff}=3.0–4.0 eV (for LDA) to give the best overall description for the energetics, lattice constant, and magnetic ordering in Ce_2O_3. Castleton et. al. [25] investigated $Ce4f$ electron localization and suggested the best choice for U_{eff} to be 6.0 eV for LDA and 5.5 eV for PBE. Overall, the published studies that consider both CeO_2 and Ce_2O_3 cover the range of U_{eff} parameter between 2 and 8 eV, depending on the property of interest [22, 25, 29, 30, 38].

In the present contribution we explore DFT+U approach with the most popular LDA, PBE and PW91 exchange-correlation functionals using previously suggested values of U_{eff} to find the most reasonable description of oxygen vacancies formation energies in nanoceria. The spin densities are used to analyze the degree of electron localization, closely related to U_{eff} value. Experimentally measured energies of oxygen vacancies formation in both bulk and nanoparticles are used as a reference [15–17].

Computational details

All calculations were carried out with the plane-wave based Vienna ab initio simulation package (VASP) [39, 40]. The geometry optimization of electronic ground state was performed using local density (LDA+U) approximation. On-site Coulomb and exchange interaction are treated by a single effective parameter $U_{eff} = U\text{-}J$. We used plane waves energy cutoff of 415 eV, projected augmented wave (PAW) method, and U_{eff}=5 eV [41]. These calculation parameters were recently employed for investigation of defect formation in ceria nanoparticles [34, 35]. We adopt computational protocol from these papers to investigate the effect of exchange correlation functional and the choice of U_{eff} value on the electron distribution and thermodynamic predictions.

The selection of model nanoparticle structure is critical for the reliability of computed observables. In this investigation we selected nanoparticles of octahedral shape constructed by (111) planes cut from the bulk fluorite CeO_2 lattice. These nanoparticles with chemical formula $Ce_{19}O_{32}$ and $Ce_{44}O_{80}$ are presented in Fig. 1. Our assumption of

Fig. 1 Investigated octahedral ceria nanoparticles which are cut from the bulk fluorite CeO_2 by (111) planes: (a) $Ce_{19}O_{32}$, and (b) $Ce_{44}O_{80}$
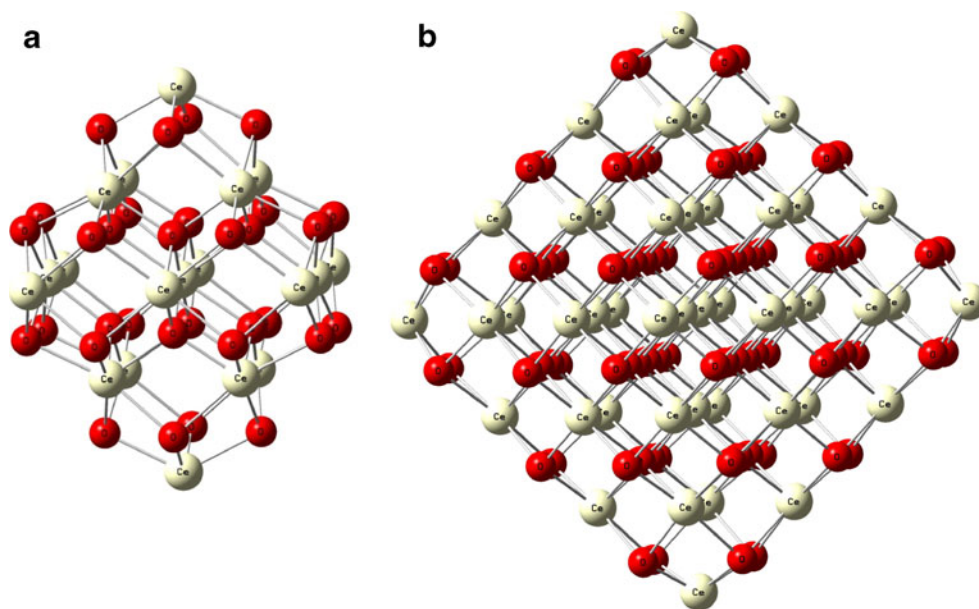
thermodynamic stability of octahedral nanoceria is consistent with preferential stability of (111) surface of CeO_2 [42]. The choice of these model nanostructures is also in line with experimental findings that report truncated octahedral shape for smaller nanoparticles (3–10 nm) and the octahedral shape for the larger ones [43, 44].

Recently Loschen et al. performed a versatile investigation of structural and energetic properties of a number of nanoceria structures with both octahedral and truncated octahedral shapes [35]. They demonstrated that among small clusters the stoichiometric moiety $Ce_{13}O_{26}$ is the most stable one. The disadvantage of this system is the absence of Ce^{3+} ions, making it a poor model to study nanoceria. For instance, the lattice constant increase for smaller nanoparticles (known as the lattice anomaly), is observed for oxygen deficient nanoparticles, but not for stoichiometric ones [45]. In this study we used symmetric octahedral non-stoichiometric nanoparticles based on the fact that essential properties of moderately large ceria nanoparticles were adequately reproduced by using bulk-derived octahedral models [34, 35].

The vacancy formation energy was calculated as:

$$E_{vac} = \left(E_{def} + \frac{1}{2}nE_{O_2} - E_{perf} \right)/n, \qquad (1)$$

where E_{perf} and E_{def} are the total energies of the structures before and after the formation of n vacancies and E_{O_2} is the energy of the oxygen molecule. The energies E_{def} and E_{perf} were obtained in calculations of the relaxed structures, and the energy E_{O_2} was obtained in spin-polarized calculations of the O_2 molecule in periodical box with the side of 10 Å in length.

Results and discussion

Defect formation energies

The values of E_{vac} for bulk, CeO_2 (111) slab and octahedral nanoparticles $Ce_{19}O_{32}$ and $Ce_{44}O_{80}$ calculated in the present work are summarized in Table 1 and compared with available results from the literature. As one can see, our PW91+U results (U_{eff}=3 eV) for optimized $Ce_{19}O_{32}$ and $Ce_{44}O_{80}$ nanoparticles confirm the results of Loschen et al. [35]. The surface oxygen vacancy formation energies obtained with LDA+U and GGA+U noticeably differ, while both PW91 and PBE functionals give very close results at the same values of U_{eff}. For this reason we focused our attention on LDA and PBE functionals only.

Next we investigated the effect of parameter U_{eff} on the binding energy of $Ce_{44}O_{80}$ ceria nanoparticle calculated with PBE exchange-correlation functional using equation

$$E_b = \frac{E(Ce_{n_{Ce}}O_{n_O}) - (n_{Ce}\mu_{Ce} + 1/2n_O\mu_{O_2})}{n_{Ce} + n_O}, \qquad (2)$$

where n_{Ce} and n_O are the number of Ce and O atoms in ceria nanoparticles and μ_{Ce} and μ_{O_2} are chemical potentials of cerium and oxygen atoms, respectively. The μ_{Ce} was calculated for γ-Ce and μ_{O_2} is the chemical potential of the oxygen molecule in the gas phase. Results are presented in Fig. 2a. In contrast to bulk ceria, where formation energies of both crystal modifications of ceria slightly increase with U_{eff}, the absolute value of E_b of nanoceria steadily decreases. In other words, theory predicts less stable ceria nanoparticle as U_{eff} grows. The minimum appearing on the $E_b(U_{eff})$ curve coincides with the minima in formation

Table 1 Oxygen vacancy formation energy

System	Method	U_{eff}, eV	V_O position	E_{vac}, eV
Bulk CeO_2	LDA+U_{eff}	5	Inside	4.35[a]
	PW91	0	Inside	4.73[b]
	PW91+U_{eff}	5	Inside	4.55[c]
	FP-LMTO-PW91	–	Inside	4.55[d]
	Experiment	–	Inside	4.67[e]
(111) CeO_2 surface	LDA+U_{eff}	5	Surface	3.33[a]
	LDA+U_{eff}	5.3	Surface	3.21–3.31[f]
	PW91	0	Surface	3.39[b]
	PW91+U_{eff}	3	Surface	3.91[a]
	PBE+U_{eff}	4.5	Surface	2.34–2.50[f]
	PW91+U_{eff}	5	Surface	2.60[c]
			Surface/subsurface	2.13/1.94[g]
$Ce_{19}O_{31}$	LDA+U_{eff}	5	Surface/ inside	1.92[a]
	PW91+U_{eff}	3	Surface/ inside	3.55/ 4.31[h]
	PBE+U_{eff}	2	Surface/ inside	5.14[a]
		5.5	Surface/ inside	3.44[a]
		7	Surface/ inside	0.70[a]
$Ce_{19}O_{30}$	LDA+U_{eff}	5	Surface	3.29[a]
	PW91+U_{eff}	3	Surface	4.54[a]
	PBE+U_{eff}	2	Surface	4.42[a]
		5.5	Surface	3.71[a]
		7	Surface	2.45[a]
$Ce_{44}O_{79}$	LDA+U_{eff}	5	Surface	0.72[a]
	PW91+U_{eff}	3	Surface	3.52[h]
	PBE+U_{eff}	2	Surface	5.19[a]
		5.5	Surface	−0.62[a]
		7	Surface	−2.07[a]
$Ce_{44}O_{78}$	LDA+U_{eff}	5	Surface	1.97[a]
	PW91+U_{eff}	3	Surface	4.52[a]
	PBE+U_{eff}	2	Surface	4.49[a]
		5.5	Surface	0.93[a]
		7	Surface	−1.09[a]
$Ce_{44}O_{77}$	LDA+U_{eff}	5	Surface	2.36[a]
	PW91+U_{eff}	3	Surface	3.73[a]
	PBE+U_{eff}	2	Surface	4.21[a]
		5.5	Surface	1.41[a]
		7	Surface	0.36[a]
$Ce_{44}O_{76}$	LDA+U_{eff}	5	Surface	1.92[a]
	PBE+U_{ef}	2	Surface	4.16[a]
		5.5	Surface	1.73[a]
		7	Surface	1.12[a]
$Ce_{85}O_{159}$	LDA+U_{eff}	5	Surface	0.54[a]
Nanocrystalline	Experiment	–	Extrinsic (grain boundary)	1.18–1.52[i]
	Experiment	–	Intrinsic (inside grain)	1.77–2.28[i]

[a] This work; [b] Ref. [47]; [c] Ref. [36]; [d] Ref. [48]; [e] Ref. [49]; [f] Ref. [50]; [g] Ref. [51]; [h] Ref. [35]; [i] Refs. [15–17].

energies obtained for both modifications of ceria and corresponds to delocalization of f-electrons at U_{eff}<2 eV accompanied by Mott transition (collapse of electronic solution for the γ-Ce to solution for α-Ce with itinerant f electrons) [22].

Increase of E_b leads to decrease of E_{vac} for one vacancy formation (Fig. 2b). For U_{eff}>5.3 eV, $Ce_{44}O_{80}$ becomes unstable with respect to one surface oxygen vacancy formation. At U_{eff}=2 eV predicted value of E_{vac} is 5.19 eV, that is larger than experimental value of oxygen
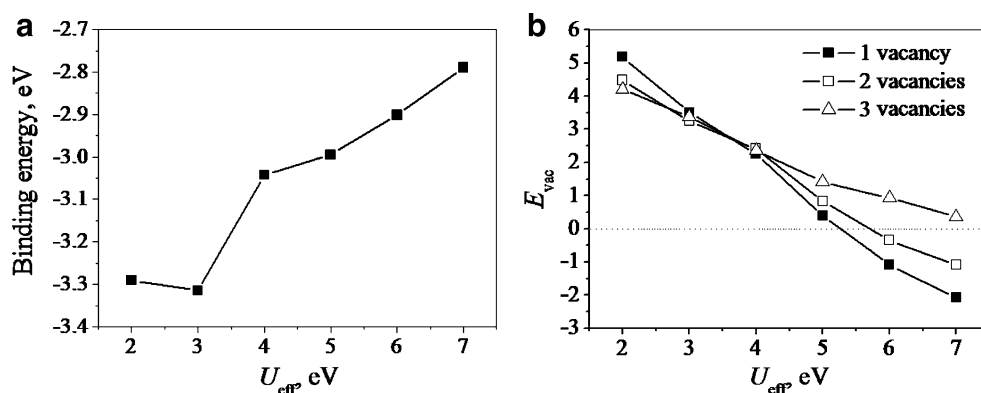
vacancy formation in bulk ceria. Energies per one vacancy required to remove two or three surface oxygen atoms at U_{eff}=2 eV are equal to 4.49 and 4.21 eV, respectively. These data are also close to E_{vac} in bulk and seem to be overestimated. On the other hand, at U_{eff}<3.5 eV the energy cost of creating multiple oxygen vacancies becomes smaller. On the other hand, at U_{eff}>3.5 eV the $Ce_{44}O_{80}$ nanoparticle becomes more stable with respect to formation of two and three surface oxygen vacancies. The $Ce_{19}O_{32}$ nanoparticle demonstrates the same trend to increase E_{vac} with more surface vacancies formation, while the values of E_{vac} are significantly larger than for the $Ce_{44}O_{80}$ one.

To summarize all calculated data for both considered ceria nanoparticles, we plot the E_{vac} as a function of $x=N_{Ce3+}/N_{Ce}$ calculated with different U_{eff} in Fig. 3. N_{Ce3+} and N_{Ce} are the number of Ce^{3+} cations and total number of Ce atoms in the nanoparticle, respectively. The function $E_{vac}(x)$ is not monotonic at small (c.a. 2 eV), and large (c.a 7 eV) values of U_{eff}, while at U_{eff}=5.5 eV it is steadily increasing. Such behavior could be explained by the effect of f-electrons localization. As it was demonstrated in [25], f-electrons localization is described very well using PBE functional with U_{eff}=5.5 eV while at U_{eff}=2 and 7 eV their delocalization is significant. This peculiarity is reflected in non-monotonic $E_{vac}(x)$ behavior. Slope of $E_{vac}(x)$ at the values of U_{eff}=2 and 7 eV is opposite: $E_{vac}(x)$ at smaller U_{eff} decreases, $E_{vac}(x)$ at larger U_{eff} increases. At the value of U_{eff}=5.5 eV behavior of $E_{vac}(x)$ represents an intermediate case of monotonic function. In the following, all the properties will be discussed assuming this value. At that value E_{vac} per one vacancy decreases with (i) decrease of number of introduced oxygen vacancies and (ii) nanoparticle size increase. The only parameter that is common for both of these characteristics is Ce^{3+}/Ce^{4+} ratio. In other words, E_{vac} decreases with Ce^{3+}/Ce^{4+} ratio decrease.

At low Ce^{3+}/Ce^{4+} ratio it is easy to create vacancy and ceria nanoparticle is unstable while at large Ce^{3+}/Ce^{4+} ratio E_{vac} exceeds some critical value where oxygen atom cannot be removed even under strong reduction conditions. Using results for $Ce_{44}O_{80-n}$ nanoparticle we estimate the equilib-

rium concentration of Ce^{3+} to be about 45–55%. This is more than twice as large as experimentally evaluated concentration for Ce^{3+} ions of ~18% ceria nanoparticle of 3 nm diameter [46]. This discrepancy could be explained by a smaller size of the model nanoparticle, neglecting environmental effects (aqueous solution), and neglected structural details (truncated octahedral shape of ceria nanoparticles of less than 10 nm in diameter). Removing vertex Ce ions would allow to fine tune Ce^{3+}/Ce^{4+} ratio and may be used to improve description of nanoceria energetics.

Spatial distribution of spin density

The vacancy formation thermochemistry, discussed in the previous section is closely related to the f electron localization on certain cerium atoms. The preferable spatial distribution of Ce^{3+} and Ce^{4+} cations on the surface and interior of ceria nanoparticles can also be important for catalytic activity of ceria. In order to analyze these details of electron structure, we plotted spin distribution obtained for $Ce_{44}O_{80}$ and $Ce_{44}O_{79}$ nanoparticles on Fig. 4. We optimized the structure in spin polarized approach and identified the oxidation state of Ce using the magnetic
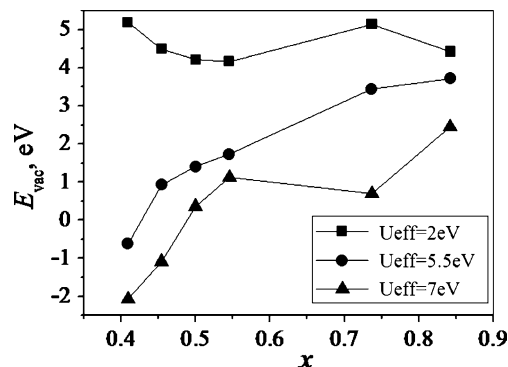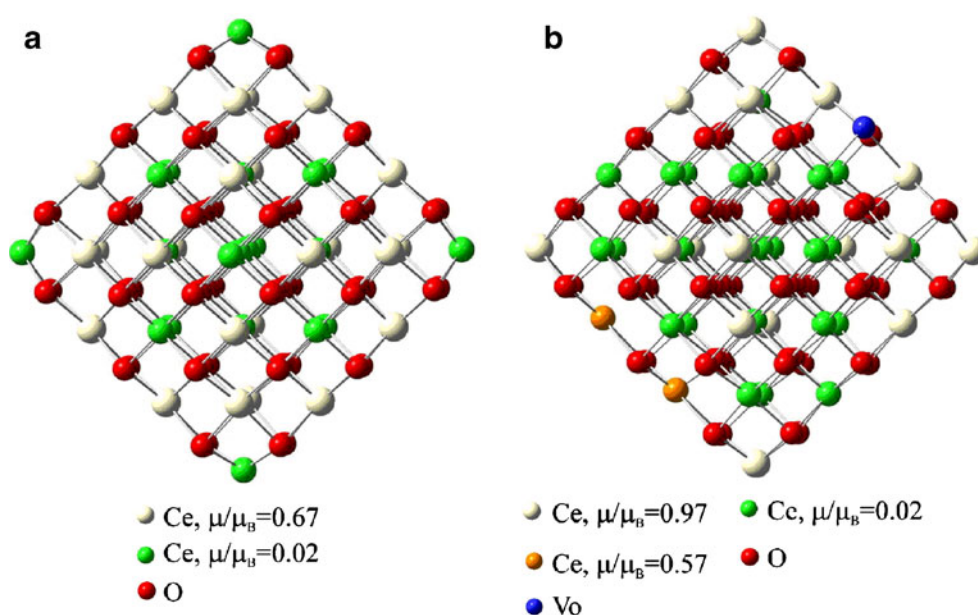

Fig. 3 PBE+U_{eff} calculated values of E_{vac} as a function of $x=N_{Ce3+}/N_{Ce}$, where N_{Ce3+} and N_{Ce} are the number of Ce^{3+} cations and total number of Ce in ceria nanoparticle, respectively

Fig. 4 Spin distribution in (**a**) $Ce_{44}O_{80}$ and (**b**) $Ce_{44}O_{79}$ ceria nanoparticles

moment at Ce atoms as an indicator. Results for $Ce_{44}O_{80}$ are in perfect agreement with the predictions recently reported by Loschen et al. [35]. The paramagnetic Ce^{4+} ions occupy inside, facet, and corner sites while edge cations are in delocalized ferromagnetic spin state with magnetic moment of $0.67\,\mu_B$ (Fig. 4a).

The introduction of one surface vacancy drastically changes spin density distribution. As shown in Fig. 4b, all Ce cations at corner sites (except one) increase their magnetic moment to $0.97\,\mu_B$, while the edge opposite to the facet with vacancy has two Ce atoms with magnetic moment equal to $0.57\,\mu_B$, sharing f-electron.

The geometry optimization at spin polarized level was reported [35] to be critically important for the spatial distribution of Ce^{3+}/Ce^{4+} cations in $Ce_{19}O_{32}$ nanoparticle. On the other hand for $Ce_{44}O_{80}$ nanoparticle there is no difference in spin distributions calculated using geometries optimized at spin polarized or spin restricted levels. We performed spin polarized geometry optimization for octahedral shaped $Ce_{85}O_{160}$ and found [35] that spatial spin distribution differs from the one predicted for structure optimized with spin restricted calculations. There are 6 corner, 36 edge, 24 facet and 19 internal Ce sites in $Ce_{85}O_{160}$ nanoparticle. For structure optimized using spin restricted level of theory, the corner and edge Ce cites possess magnetic moments of 0.70 and $0.41\,\mu_B$ respectively, while magnetic moments at all other sites are zero. In the case of structure optimized with spin polarized approach, there are magnetic moment of $0.97\,\mu_B$ localized at corner sites and $0.62\,\mu_B$ on 24 out of 36 edge sites. The value of magnetic moment does not exceed $0.02\,\mu_B$ on all remaining Ce cations.

Conclusions

We reported the DFT+U predictions for oxygen vacancy formation energy and spin distribution in model ceria nanoparticles. All systems were relaxed at LDA+U_{eff} (U_{eff}=5 eV) level of theory [22, 34, 35]. Energy of oxygen vacancies formation was evaluated using LDA, PBE, and PW91 exchange-correlation functionals and different on-site correlation energies U_{eff}. We found that previously recommended values of U_{eff}=3 eV for PW91 functional and U_{eff}=2 eV for PBE one reproduce E_{vac} for bulk ceria well, while for nanoceria calculated values of oxygen vacancy formation energy are significantly overestimated. LDA+U_{eff} approach gives better agreement with experiment for nanoceria due to fortuitous error cancellation [22]. At PBE+U_{eff} level we found that decreasing of U_{eff} parameter increases the value of E_{vac}, and the best agreement with experiment on both bulk and nanoceria is obtained with U_{eff}=5.5 eV, previously proposed by Castleton et. al. on the basis of different arguments (Ce4f states localization) [25]. We also established that creation of one surface vacancy in $Ce_{44}O_{80}$ nanoparticle leads to significant spin redistribution. In the case of $Ce_{85}O_{160}$ the structures optimized at spin restricted or spin polarized level of theory resulted in different surface spin distribution.

References

1. Kaspar J, Fornasiero P, Graziani M (1999) Catal Today 50: 285–298
2. Steele BCH, Heinzel A (2001) Nature 414:345–352
3. Chen JP, Patil S, Seal S, McGinnis JF (2006) Nat Nanotechnol 1:142–150
4. Duclos SJ, Vohra YK, Ruoff AL, Jayaraman A, Espinosa GP (1988) Phys Rev B 38:7755–7758
5. Barnighausen H, Schiller G (1985) J Less-Common Met 110:385–390
6. Kang ZC, Eyring L (1998) Oxides. Trans Tech, Clausthal Zellerfe, pp 301–358
7. Heinemann C, Cornehl HH, Schroder D, Dolg M, Schwarz H (1996) Inorg Chem 35:2463–2475
8. Seal S, Shukla S (2002) In: Baraton M, Nalwa HS (eds) Functionalization and surface treatment of nanoparticles. Academic, San Diego, CA
9. Herman GS (1999) Surf Sci 437:207–214
10. Suzuki T, Kosacki I, Anderson HU, Colomban P (2001) J Am Ceram Soc 84:2007–2014
11. Mamontov E, Egami T, Brezny R, Koranne M, Tyagi S (2000) J Phys Chem B 104:11110–11116
12. Conesa JC (1995) Surf Sci 339:337–352
13. Tsunekawa S, Sahara R, Kawazoe Y, Ishikawa K (1999) Appl Surf Sci 152:53–56
14. Deshpande S, Patil S, Kuchibhatla SVNT, Seal S (2005) Appl Phys Lett 87:133113-1–133113-3
15. Chiang YM, Lavik EB, Kosacki I, Tuller HL, Ying JY (1996) Appl Phys Lett 69:185–187
16. Chiang YM, Lavik EB, Blom DA (1997) Nanostructured Mater 9:633–642
17. Chiang YM, Lavik EB, Kosacki I, Tuller HL, Ying JY (1997) J Electroceram 1:7–14
18. Skorodumova NV, Ahuja R, Simak SI, Abrikosov IA, Johansson B, Lundqvist BI (2001) Phys Rev B 64:115108
19. Fabris S, de Gironcoli S, Baroni S, Vicario G, Balducci G (2005) Phys Rev B 71:041102
20. Kresse G, Blaha P, Da Silva JLF, Ganduglia-Pirovano MV (2005) Phys Rev B 72:237101
21. Fabris S, de Gironcoli S, Baroni S, Vicario G, Balducci G (2005) Phys Rev B 72:237102
22. Loschen C, Carrasco J, Neyman KM, Illas F (2007) Phys Rev B 75:035115
23. Anisimov VI, Zaanen J, Andersen OK (1991) Phys Rev B 44:943–954
24. Anisimov VI, Korotin MA, Zaanen J, Andersen OK (1992) Phys Rev Lett 68:345–348
25. Castleton CWM, Kullgren J, Hermansson K (2007) J Chem Phys 127:244704
26. Pederson MR, Heaton RA, Lin CC (1985) J Chem Phys 82: 2688–2699
27. Perdew JP, Zunger A (1981) Phys Rev B 23:5048
28. Hay PJ, Martin RL, Uddin J, Scuseria GE (2006) J Chem Phys 125:034712
29. Da Silva JLF, Ganduglia-Pirovano MV, Sauer J, Bayer V, Kresse G (2007) Phys Rev B 75:045110-045121
30. Andersson DA, Simak SI, Johansson B, Abrikosov IA, Skorodumova NV (2007) Phys Rev B 75:035106-035109
31. Cococcioni M, de Gironcoli S (2005) Phys Rev B 71:035105
32. Fabris S, Vicario G, Balducci G, de Gironcoli S, Baroni S (2005) J Phys Chem B 109:22860–22867
33. Jiang Y, Adams JB, van Schilfgaarde M (2005) J Chem Phys 123:1949189
34. Loschen C, Bromley ST, Neyman KM, Illas F (2007) J Phys Chem C 111:10142–10145
35. Loschen C, Migani A, Bromley ST, Illas F, Neyman KM (2008) Phys Chem Chem Phys 10:5730–5738
36. Nolan M, Grigoleit S, Sayle DC, Parker SC, Watson GW (2005) Surf Sci 576:217–229
37. Dudarev SL, Botton GA, Savrasov SY, Szotek Z, Temmerman WM, Sutton AP (1998) Phys Status Solidi A 166:429–443
38. Jiang Y, Adams JB, van Schilfgaarde M, Sharma R, Crozier PA (2005) Appl Phys Lett 87:2084324
39. Kresse G, Hafner J (1993) Phys Rev B 47:558–561
40. Kresse G, Furthmuller J (1996) Phys Rev B 54:11169–11186
41. Blochl PE (1994) Phys Rev B 50:17953–17979
42. Skorodumova NV, Baudin M, Hermansson K (2004) Phys Rev B 69:075401
43. Yang SW, Gao L (2006) J Am Chem Soc 128:9330–9331
44. Chen MY, Zu XT, Xiang X, Zhang HL (2007) Physica B 389:263–268
45. Tsunekawa S, Fukuda T, Kasuya A (2000) Surf Sci 457: L437–L440
46. Dutta P, Pal S, Seehra MS, Shi Y, Eyring EM, Ernst RD (2006) Chem Mater 18:5144–5146
47. Yang ZX, Woo TK, Baudin M, Hermansson K (2004) J Chem Phys 120:7741–7749
48. Skorodumova NV, Simak SI, Lundqvist BI, Abrikosov IA, Johansson B (2002) Phys Rev Lett 89:166601
49. Tuller HL, Nowick AS (1979) J Electrochem Soc 126:209–217
50. Ganduglia-Pirovano MV, Da Silva JLF, Sauer J (2009) Phys Rev Lett 102:026101–026104
51. Li H-Y, Wang H-F, Gong X-Q, Guo Y-L, Guo Y, Lu G, Hu P (2009) Phys Rev B 79:193401–193404